Research Article

Effect of the AgO_2 doping on the superconducting material of $YAg_xBa_2Cu_3O_{7-\delta}$, $Y_3Ag_xBa_5Cu_8O_{18-\delta}$ and $Y_7Ag_xBa_{11}Cu_{18}O_{40-\delta}$

Somkid Sinwittayarak[1], Supphadate Sujinnapram[2], Tunyanop Nilkamjon[3], Sermsuk Ratreng[3], Pongkaew Udomsamuthirun[3], Suppanyou Meakniti[4] and Thitipong Kruaehong[5]*

Received: 18 February 2024
Revised: 16 April 2024
Accepted: 18 April 2024

ABSTRACT

The Y123, Y358, and Y7-11-18, and AgO_2 composite was predominantly synthesized through a solid-state reaction. As the Ag content increased, both the critical temperature and the superconducting compound exhibited enhancement. The non-superconducting compound segregated into two distinct groups: $BaCuO_2$ (Im-3m) and $Ba_2Cu_3O_6$ (Pccm). While Ag doping did not impact the *c* lattice parameter value, it did alter the *a* and *b* lattice parameters in Y358 and Y7-11-18. Y123 demonstrated the most stable anisotropic parameters. Additionally, Ag doping did not influence the increase in oxygen content. Among the samples, Y123 exhibited the highest Cu^{3+}/Cu^{2+} ratio, while Y7-11-18 displayed the most deficient parameters, contributing to a higher critical temperature. The heat reaction for all samples indicated an endothermic reaction, resulting in a decrease in the samples' melting point. Furthermore, compared to undoped samples, Ag doping enhanced the surface homogeneity.

Keywords: Electrical resistivity, Ag composite, Solid state reaction

[1] Department of Computer Science, Faculty of Science and Technology, Suratthani Rajabhat University, Suratthani 84100, Thailand.
[2] Department of Physics, Faculty of Liberal Arts and Science, Kasetsart University, Kamphaeng Saen Campus, Nakhon Pathom 73140, Thailand.
[3] Prasanmitr Physics Research, Department of Physics, Faculty of Science, Srinakharinwirot University, Bangkok 10110, Thailand.
[4] Department of General Science, Faculty of Education, Suratthani Rajabhat University, Suratthani 84100, Thailand.
[5] Department of Industrial Electrics, Faculty of Science and Technology, Suratthani Rajabhat University, Suratthani 84100, Thailand.
*Corresponding author, email: thitipong.kru@sru.ac.th

Introduction

To improve the superconductivity state of YBaCuO ceramic, it is necessary to add a metallic element to the crystal structure. The mechanism of oxide superconductors depends on the distribution of the $3d^9$ configuration in Cu^{2+} and the $3d^8$ configuration in Cu^{3+} in the octahedral structure [1]. Intensive research for higher critical temperature by replacing Y^{3+} with La^{3+} in La214 (La_2BaCuO_4), the first cuprate superconducting material discovered by Bednorz and Muller [2], which has a critical temperature of 35 K. Since Y^{3+} has an ionic radius smaller than La^{3+} in the perovskite structure, Y123 ($YBa_2Cu_3O_7$) has a critical temperature higher than La214, with a critical temperature of 93 K discovered by Chu and Coworkers [3] in 1987. The two superconductors have a very different critical temperature: Y123 has become one of the most promising for many potential applications, with a critical temperature of 58 K. Considering the crystal structure of Y123, it has one Cu-O chain and two CuO_2 planes [4] with lattice constants of a=3.8286 Å, b=3.8873 Å, and c=11.6938 Å [5]. Recently, the new ceramic superconductor Y358 ($Y_3Ba_5Cu_8O_{18-\delta}$) [6] with a critical temperature above 102 K and lattice parameters of a=3.888 Å, b=3.823 Å, and c=31.013 Å was found. The difference in critical temperature between Y123 and Y358 is about 9 K, with Y358 having the highest critical temperature of any YBaCuO family. In 2010, Tavana et al [7] analyzed the crystal structure of Y358, revealing that it has three Cu-O chains and five CuO_2 planes with a space group of Pmm2 symmetry. In 2012, Gholipour et al [8] synthesized the Y358 compound using the solgel technique. The crystal structure of Y358 has 6 CuO_2 and 2 Cu-O chains with Pmmm symmetry and lattice parameters of a= 3.845 Å, b= 3.895 Å, and c= 31.070 Å. Khosroabadi et al [9] analyzed the crystal structure of Y358 in 2014, finding lattice parameters of a= 3.838 Å, b= 3.904 Å, and c= 31.043 Å with 6 CuO_2 planes and 2 Cu-O chains. Y358 consists of two Y123 unit cells and one block of the second phase of Y123, which is Y211 (Y_2BaCuO_5), between Y123. The enhancement of the critical current density (J_c) [10], critical magnetic field (H_c) [11], and increasing the critical temperature are related to doping [12]. The first synthesis of YBaCuO was done by solid-state reaction, and the material was a stable solid state material. Addition or substitution is very important and effective in controlling and improving the crystal structure. YBaCuO ceramic superconductors have the Cu-O planes arranged in CuO_2 planes, which is a component factor for carrying the reservoirs. Therefore, selecting elements that may replace Cu ion in the structure of YBaCuO material to improve the superconducting properties is essential. In the periodic table, copper and silver are from the same group; Ag can substitute Cu and can affect the microscopic granularity. The difference in atomic radius between Cu=1.45 Å and Ag=1.65 Å is close. In 2005, Li et al [13] improved the current density of the thin film of Y123 by doping Ag. The inclusion of Ag, the liquid silver, fills into the inhomogeneous surface and modifies the structure, thus strengthening the role of pinning centers for high current applications.

The new approach for synthesizing the new YBaCuO family was discovered by Udomsamuthirun et al [14] in 2010. The sum of Ba-atoms and Y-atoms equals the number of Cu-atoms. The new YBaCuO family consists of Y3-8-11 ($Y_3Ba_8Cu_{11}O_y$), Y5-8-13 ($Y_5Ba_8Cu_{13}O_y$), Y7-11-18 ($Y_7Ba_{11}Cu_{18}O_y$), and Y13-20-33 ($Y_{13}Ba_{20}Cu_{33}O_y$). In their results, Y7-11-18 showed a sharp critical temperature curve, with

the lowest value of the anisotropic parameter indicating that Y7-11-18 tends to be a good superconductor. The new Y-based material has Y-atoms missing per Ba-atoms. The critical temperature and XRD pattern are closely related to Y123. Therefore, the new YBaCuO material has lattice parameters close to Y123. Sujinnapram et al [15] repeated the characterization of the lattice parameters and phase composition in the new YBaCuO material using the Rietveld refinement software program [16]. The results revealed that the samples have a superconducting phase and a non-superconducting phase. The superconducting phase has an orthorhombic structure with Pmmm space group, and the non-superconducting phase has Y211 (Y_2BaCuO_5) with Pbnm and Pnma space groups, $BaCuO_2$ with Im-3m space group, and $Ba_2Cu_3O_6$ with Pccm space group. The new YBaCuO family has a linear *c*-axis following Cu-atoms. However, the *c* lattice parameter is longer following Y-atoms. Nevertheless, the critical temperature values are close to Y123, and the surface morphology is inhomogeneous.

In this study, we investigated the effect of Ag doping on Y123, Y358, and Y7-11-18 superconductors with doping values x = 0, 0.1, and 0.2 mole concentrations, respectively. The samples were synthesized using the solid-state reaction technique. The samples were characterized by ρ−T analysis, the structural patterns were analyzed using power X-ray diffraction and High X, Pert, which was approved by the Fullprof software program. The ratio of Cu^{3+}/Cu^{2+}, oxygen content, and deficiency parameters was determined using the iodometric titration method, while the melting point temperature and heat reaction were investigated using Differential Thermal Analysis (DTA). Finally, the surface morphology and elemental analysis were characterized using Energy Dispersive X-ray Spectroscopy (EDX).

Experimental Procedure

The series of samples, $YAg_xBa_2Cu_3O_{7-\delta}$, $Y_3Ag_xBa_5Cu_8O_{18-\delta}$, and $Y_7Ag_xBa_{11}Cu_{18}O_{40-\delta}$, with silver content concentrations of x = 0, 0.1, and 0.2 moles, were synthesized using the solid-state reaction method. High-impurity Y_2O_3, $BaCO_3$, CuO, and AgO_2 served as starting chemicals. All samples were weighed in stoichiometric proportions, mixed, and ground in an agate mortar and pestle. The starting powders underwent heat treatment by calcination in air at 950 °C. After 24 hours of holding at the peak temperature, the powder was cooled to room temperature. The calcination process was repeated twice with intermediate grinding. The weighed precursor was then formed into pellets with a diameter of 30 mm and a thickness of 3 mm using a 2,000psi uniaxial pressure. Subsequently, the samples obtained were sintered at 950 °C for 24 hours and subjected to final heating, and annealed at 500 °C for 24 hours in air. After sintering and annealing, the samples resulted in pellets with an approximate diameter of 30 mm.

The pellet samples were analyzed using various techniques. The properties of the samples were investigated using a d.c. four-point probe measurement method, which involved measuring electrical conductivity in a liquid nitrogen bath with a Fluke 8845A digital multimeter. The probes of the samples were in contact with epoxy-silver paint. Measurements were conducted in the temperature range of 77 K to 120 K with a current density of 2.55×10^{-3} A/m^2. Temperature measurements were performed using a type K thermocouple attached to the center of the specimens. The critical measurements of the pellets

were carried out using the four-probe method at room temperature in the milliohm range. For current-voltage measurements, the distance between the two current contacts was fixed at 5 mm for all samples. Powder X-ray diffraction techniques were performed at room temperature using a D8 Discovery diffractometer with CuKα radiation to characterize the crystal structure. The lattice parameters of phase composition, space group, and anisotropic parameters were analyzed using the FULLPROF software refinement program. Microstructural observation and chemical compositional analysis were conducted using an FEI Quanta 400 with a high voltage of 20 kV, and energy-dispersive X-ray spectroscopy (EDX) with electron microanalysis-elemental mapping analysis attached to the SEM. Iodometric titration measurements characterized the ratio of Cu^{3+}/Cu^{2+}, deficiency parameters (δ), and oxygen content. The Perkin Elmer DTA7 determined the melting point temperature and heat reaction. Finally, EDX mapping techniques were used to examine the surface morphology and elementary analysis.

Results and discussions

In Figures 1-3 depict the normal resistivity versus temperature curves of the samples. The blue curve represents pure Y123, Y358, and Y7-11-18, while the red and black curves represent Ag doping at 0.1 and 0.2 mole concentrations, respectively. The pure samples exhibit the lowest $T_c$offset and $T_c$onset. Both $T_c$offset and $T_c$onset shift with increased Ag doping, resulting in higher values for the pure samples. The $T_c$onset and $T_c$offset values are presented in Table 1. The maximum critical temperature onset ($T_c$onset) for 0.2 mole concentration in Y123, Y358, and Y7-11-18 is found to be 92.96 K, 95.94 K, and 98.01 K, respectively. Furthermore, the empirical formula of Y123, Y358, and Y7-11-18 ceramics indicates that substitution of silver ions at the Copper ion site and the creation of electron holes are crucial for superconductivity. Additionally, the substitution of Ba^{2+} ions at Y^{3+} sites optimizes the critical temperature, approaching 93 K [17]. The electron holes are generated in the CuO_6 plane [18]. However, their occurrence varies. In the pure sample, ionic bonding is limited, and the hole could be generated at the Cu atom site, leading to Cu^{2+}/Cu^{3+} mixed valence, or created at the oxygen atom site. The importance of Ag doping lies in its impact on the structural properties and critical temperature, simplifying the relation of this material.

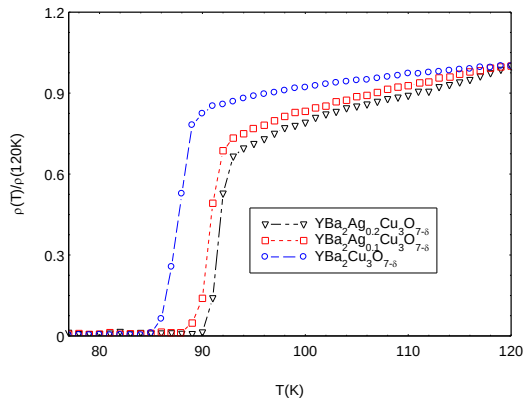

Figure 1 shows the normal resistivity versus temperature of Y123 with Ag addition.

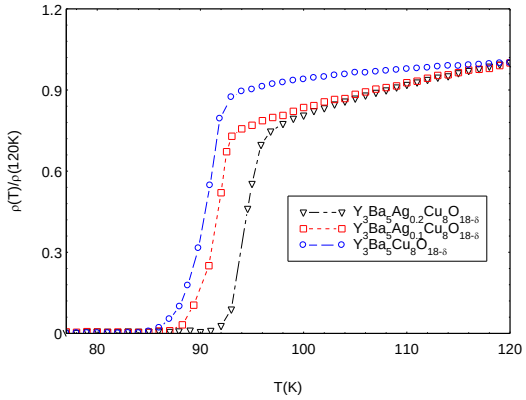

Figure 2 shows the normal resistivity versus temperature of Y358 with Ag addition.

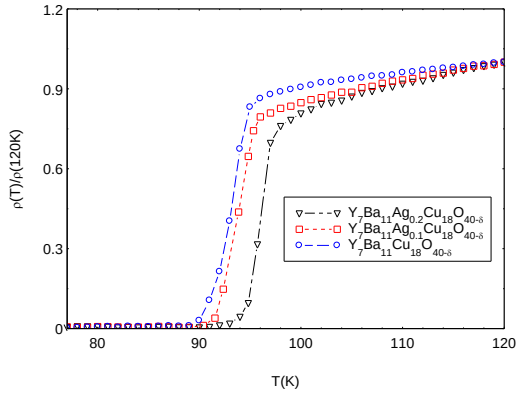

Figure 3 shows the normal resistivity versus temperature of Y7-11-18 with Ag addition.

Table 1 Critical temperature of the samples.

Samples	$T_c$offset (K)	$T_c$onset (K)
$YBa_2Cu_3O_{7-\delta}$	84.98	88.95
$YAg_{0.1}Ba_2Cu_3O_{7-\delta}$	87.88	92.00
$YAg_{0.2}Ba_2Cu_3O_{7-\delta}$	89.99	92.96
$Y_3Ba_5Cu_8O_{18-\delta}$	84.94	92.96
$Y_3Ag_{0.1}Ba_5Cu_8O_{18-\delta}$	87.02	93.04
$Y_3Ag_{0.2}Ba_5Cu_8O_{18-\delta}$	90.99	95.94
$Y_7Ba_{11}Cu_{18}O_{40-\delta}$	88.99	95.00
$Y_7Ag_{0.1}Ba_{11}Cu_{18}O_{40-\delta}$	90.39	96.01
$Y_7Ag_{0.2}Ba_{11}Cu_{18}O_{40-\delta}$	91.96	98.01

The Rietveld refinement method was used to characterize the crystal structure profile. The samples consist of two compositions: superconducting compounds and non- superconducting compounds. The non-superconducting compounds, $BaCuO_2$ and $Ba_2Cu_3O_6$, have Im-3m and Pccm space groups, respectively. The crystal structure of the superconducting compounds is orthorhombic with Pmmm symmetry space group [19]. The blue line represents pure Y123, Y358, and Y7-11-18. The red

and black solid lines represent doping with Ag at 0.1 and 0.2 mole concentrations, respectively (Figures 4-6). All spectra indicate that the samples exhibit polycrystalline behavior, and all samples have similar curve spectra.

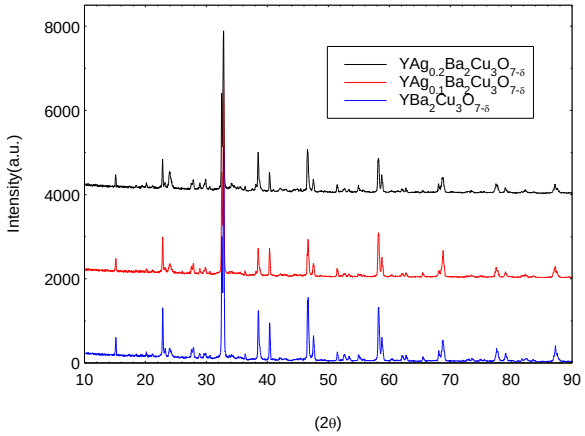

Figure 4 shows the XRD spectra of pure Y123 and Ag-doped samples.

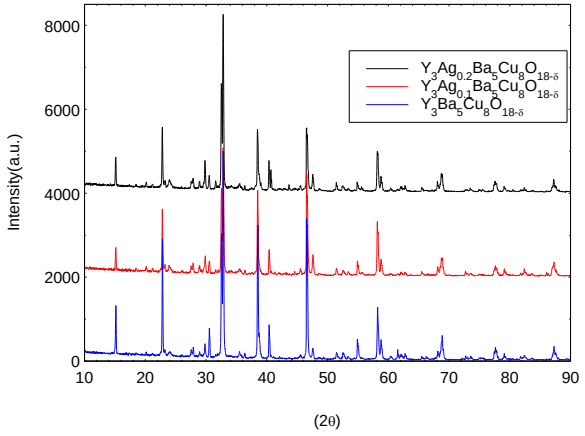

Figure 5 shows the XRD spectra of pure Y358 and Ag-doped samples.

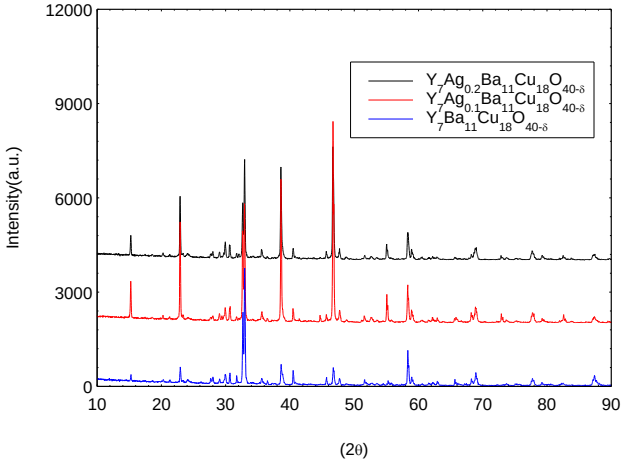

Figure 6 shows the XRD spectra of pure Y7-18-11 and Ag-doped samples.

In Figure 7, the *a*, *b*, and *c* lattice parameters of the samples resulting from the Rietveld refinement method are shown. The first figure illustrates the *a*-lattice parameter of the samples, with Y123 and Y7-11-18 represented by the blue and black solid lines, respectively. Ag doping showed no effect on these two samples. However, for Y358, the red solid line indicated a noticeable decrease in the a-lattice parameter as shown in Figure 7. The second figure displays the *b*-lattice parameter. Y123 remained invariant with Ag doping, while Y358 and Y7-11-18 exhibited minimal changes. The *b*-lattice parameters decreased with an increase in Ag content. The third figure depicts the *c*-lattice parameters versus Ag doping. Y7-11-18 had the longest *c*-lattice parameter, and Y123 had the shortest one. Ag doping has no significant effect on the three samples, resulting in straight-line curves.

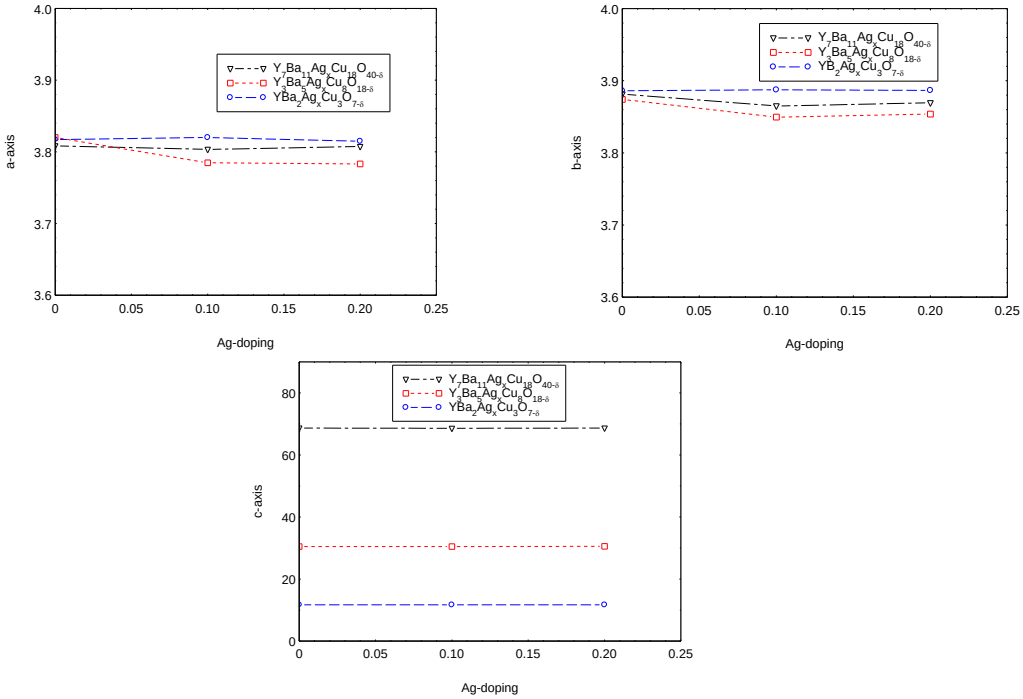

Figure 7 shows the *a*, *b*, and *c* lattice parameters of Y123, Y358, and Y7-11-18 with Ag doping.

In Figure 8, the anisotropic parameter changed significantly with Ag-doping. The blue solid line represents the Y123 sample, the red solid line represents Y358, and the black solid line represents Y7-11-18. Ag-doping had little effect on the Y123 samples but had a more pronounced effect on Y358 and Y7-11-18. As more Ag was doped into Y7-11-18, the anisotropic parameters decreased. Conversely, with an increase in Ag content, the anisotropic parameters in Y358 increased. The effect of Ag-doping on the samples varied depending on the *c*-lattice parameter. Y123 had shorter *c*-lattice parameters, while Y358 and Y7-11-18 had longer *c*-lattice parameters than Y123. The crystal structure of Y358 and Y7-11-18 changed more easily than that of Y123. The decrease in anisotropic parameters in Y7-11-18 suggests that Ag-doping can improve the structural properties of this material.

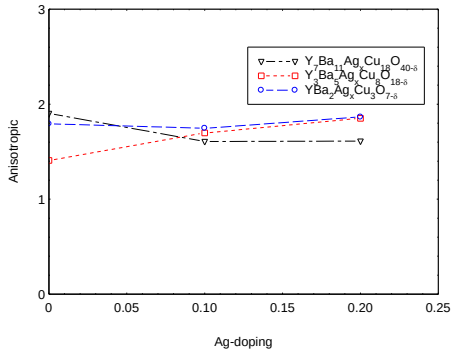

Figure 8 shows the anisotropy parameters with varying Ag-doping.

The iodometric titration method was used to determine the ratio of Cu^{3+}/Cu^{2+}, oxygen content (O_y), and deficiency parameters in the samples. Y123, Y358, and Y7-11-18 are high-temperature superconducting materials with ions of Cu^{2+} and Cu^{3+}, existing in a mixed-valence state [20]. The YBaCuO family exhibits an unstable charge, leading to the occurrence of oxygen vacancies in the crystal structure, resulting in varying oxygen content values. For Y123, Y358, and Y7-11-18, the minimum and maximum oxygen content ranged between 6.5-7, 17.5-18, and 39.5-40, respectively. The deficiency (δ) of the samples was calculated using the oxidation number method based on the oxygen content (O_y). The ratios of Cu^{2+}/Cu^{3+}, oxygen content, and deficiency are presented in Table 2. In Figure 9, the curve illustrates the relationship between the ratio of Cu^{2+}/Cu^{3+} and Ag-doping. For pure samples, Y123 exhibited the highest ratio of Cu^{2+}/Cu^{3+}, represented by the blue line. With increasing Ag-doping, Y123 showed a decrease in the ratio of Cu^{2+}/Cu^{3+} values. Regarding Y358, the ratio of Cu^{2+}/Cu^{3+} increased at 0.1 and decreased again at 0.2. For Y7-11-18, the pure sample and Ag-doping at 0.1 showed no significant changes, but when doped at 0.2, the ratio of Cu^{2+}/Cu^{3+} increased noticeably. Therefore, Ag-doping affects the Cu^{2+} and Cu^{3+} ions or Ag ions, substituting and replacing Cu atoms in the material.

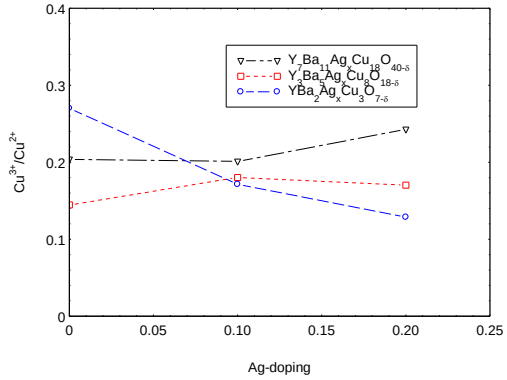

Figure 9 shows the relationship between the ratio of Cu^{3+}/Cu^{2+} and Ag-doping.

In Figure 10, the curve depicts the relationship between the oxygen constant and Ag-doping. Ag-doping did not have an effect on oxygen content; the three curves for the samples form smoothly straight lines. Y123 exhibited the lowest oxygen content, attributed to its shorter *c* lattice parameter, resulting in the lowest oxygen content in the crystal structure. The oxygen content of Y358 and Y7-11-

18 surpassed that of Y123. Y358, with more Cu-O chains and CuO_2 planes than Y123, has a higher capacity for oxygen content. Y7-11-18, with the longest *c* lattice parameter, demonstrated the maximum oxygen content. The increase in the c lattice parameter is directly related to the increase in oxygen content in the crystal structure of the samples.

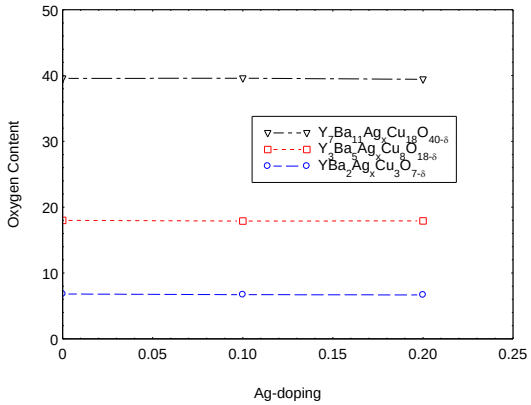

Figure 10 shows the relationship between the oxygen content value and Ag-doping.

In Figure 11, the curve illustrates the relationship between the deficiency (δ) and Ag-doping. The deficiency parameter reflected the presence of defects in the oxygen content within the crystal structure of the sample. The YBaCuO superconductors possess a complex or perovskite structure. Oxygen content deficiency arised during the high-temperature synthesis processed and due to defects in the crystal structure. The deficiency parameter was linked to the critical temperature. For Y123, δ=0 [21], indicated a non-superconducting material, and at 60 K and 90 K, δ=0.23 and δ=0.35 were observed, respectively. Increasing deficiency correlates with an elevated critical temperature in the material, as it facilitates better electron transfer by generating holes in the Cu-O chain. In pure Y123, the lowest deficiency corresponded to the lowest critical temperature. With Ag-doping, the deficiency increased, as indicated by the blue line, leading to an increase in the critical temperature. For Y358, the maximum deficiency occurs at 0.1, and at 0.2, the deficiency is lowest in pure Y358. Finally, for Y7-11-18, the deficiency is similar for the pure sample and doping at 0.1 mole concentration. However, when Ag concentration reaches 0.2 mole, the deficiency parameter significantly differed from 0 and 0.1. The critical temperature of Y7-11-18 doped at 0.2 mole concentration reached its maximum value.

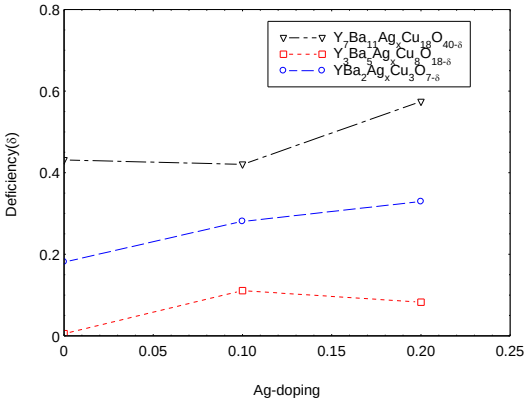

Figure 11 shows the relationship between the deficiency value and Ag-doping.

Table 2 The ratio of Cu^{3+}/Cu^{2+}, deficiency and oxygen content.

Samples	Cu^{3+}/Cu^{2+}	Deficiency (δ)	Oxygent content
$YBa_2Cu_3O_{7-\delta}$	0.2701	0.1810	6.8190
$YAg_{0.1}Ba_2Cu_3O_{7-\delta}$	0.1713	0.2806	6.7194
$YAg_{0.2}Ba_2Cu_3O_{7-\delta}$	0.1287	0.3290	6.6710
$Y_3Ba_5Cu_8O_{18-\delta}$	0.1445	0.0052	17.9948
$Y_3Ag_{0.1}Ba_5Cu_8O_{18-\delta}$	0.1802	0.1108	17.8892
$Y_3Ag_{0.2}Ba_5Cu_8O_{18-\delta}$	0.1703	0.0824	17.9176
$Y_7Ba_{11}Cu_{18}O_{40-\delta}$	0.2038	0.4311	39.5689
$Y_7Ag_{0.1}Ba_{11}Cu_{18}O_{40-\delta}$	0.2011	0.4206	39.5794
$Y_7Ag_{0.2}Ba_{11}Cu_{18}O_{40-\delta}$	0.2427	0.5741	39.4259

In Figure 12, the melting points of the samples with Ag-doping are presented. The melting points and heat reactions were investigated using Differential Thermal Analysis (Perkin Elamer DTA7) with a heating rate of 2°C/min in the temperature range of 940°C to 1200°C. In 2007, Feng et al. [22] synthesized Y123 using the solid-state reaction method, and Differential Thermal Analysis (DTA) was employed to study the thermal behavior of the samples. The samples underwent heating at a rate of 10°C/min in air. The DTA curve of the precursor powders revealed endothermic peaks during heating, with two peaks occurring at 952°C and 1022°C. Our pure samples exhibited melting points around 1030°C for Y123, 1000°C for pure Y358, and 995°C for pure Y7-11-18. The Ag-doping effect on the melting points of the samples indicated that an increase in Ag content led to a decrease in melting point temperature. The heat reactions for all samples exhibited endothermic reactions.

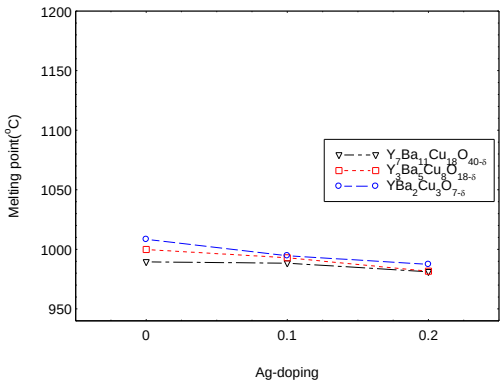

Figure 12 shows the relationship between the melting point of samples and Ag-doping.

The compositions of all samples were studied using EDX mapping techniques. The results of the EDX mapping encompassed both surface and elementary analyses simultaneously. The surfaces of the undoped samples exhibited inhomogeneous textures, and no impurities were found. The doped Ag samples showed greater homogeneity than the undoped samples. However, the micrographs of the

samples revealed different masses and orientations scattered in all directions, and microcracks between grains were observed in some samples.

In this research, we investigated the Ag-doping effects on the Y123, Y358, and Y7-11-18 bulk superconductors, focusing on their impact on the critical temperature. As the Ag content increased, the critical temperature also increased. The distinction between superconducting and non-superconducting compounds was characterized using powder X-ray diffraction. Ag-doping affected the *a* and *b* lattice parameters in Y358 and Y7-11-18, but no effect was observed in Y123. Both the Ag-doped and undoped samples exhibited equal c lattice parameters. Y123, Y358, and Y7-11-18 showed differences in anisotropy, with Y123 having the most stable anisotropic parameter. The anisotropic parameter increased in Y358, while Y7-11-18 showed a decrease with increasing Ag content. The deficiency parameter indicated defects in the oxygen content within the crystal structure of the samples. More deficiency correlated with a higher critical temperature. The oxygen content was similar across all samples. The melting point decreased with Ag doping, and the heat reaction was an endothermic reaction. The surface of undoped samples exhibited inhomogeneity, while with Ag doping, it became smoother and denser. Y123, Y358, and Y7-11-18 possess an orthorhombic structure and complex crystal structure. The metallic addition affected the physical properties, introducing distortion and creating an asymmetric structure.

Conclusions

The polycrystalline forms of Y123, Y358, and Y7-11-18, along with Ag composites with x=0, 0.1, and 0.2 mole concentrations, were synthesized by solid-state reaction. The effect of Ag doping on the samples was observed, with the critical temperature increasing as Ag content increased. The XRD results revealed an orthorhombic structure belonging to the superconducting compound with the Pmmm space group. Non-superconducting compounds were separated into two groups: $BaCuO_2$ and $Ba_2Cu_3O_6$, with Im-3m and Pccm space groups, respectively. Ag doping increased the superconducting compound and decreased the non-superconducting compound. Ag doping had no effect on the *c* lattice parameter value but changed the *a* and *b* lattice parameters in Y358 and Y7-11-18. Among the samples, Y123 exhibited the most stable anisotropic parameters. Ag doping affected the ratio of Cu^{3+}/Cu^{2+}, oxygen content, and deficiency parameters, as determined by iodometric titration techniques. Ag doping had no effect on the increased oxygen content but did affect the Cu^{3+}/Cu^{2+} ratio and deficiency parameters. Y123 showed the highest ratio of Cu^{3+}/Cu^{2+}, while Y7-11-18 exhibited the highest deficiency parameters, contributing to the highest critical temperature among the samples. The heat reaction in all samples exhibited an endothermic reaction. Ag doping resulted in a decrease in the melting point of the samples. EDX mapping techniques were employed to investigate the surface and elementary composition. Ag-doped samples showed more homogeneity than undoped samples. The micrographs of the samples revealed different masses oriented randomly in all directions, with microcracks found between grains.

Acknowledgements

The authors express gratitude for the financial support received from the Research and Development Institute of Suratthani Rajabhat University. Additionally, we wish to acknowledge the encouragement received from Prasarnmit Physics Research Unit, Department of Physics, Faculty of Science, Srinakharinwirot University.

References

1. Stern EA, Han SW, Haskel D. Dynamic inhomogeneities in the La_2CuO_4-based superconductors. J Supercond Nov Magn. 2004;17(1):97-102.
2. Bednorz JG, Muller KA. Possible high T_c superconductivity in the Ba-La-Cu-O system. Z Phy B. 1986;64:189-93.
3. Wu K, Ashburn JR, Torng CJ, Hor PH, Meng RL, Gao L, Huang ZJ, Wang YQ, Chu CW. Superconductivity at 93 K in a new mixed-phase Y-Ba-Cu-O compound system at ambient pressure. Phys Rev Lett. 1987;58;908-10.
4. Lu DH, Feng DL, Armitage NP, Shen KM, Damascelli A, Kim C, Ronning F, Shen X. Superconducting gap and strong in-plane anisotropy in untwinned $YBa_2Cu_3O_{7-\delta}$. Physical Rev Lett. 2001;86(19):4370-3.
5. Guner SB, Gorur O, Celik S, Dogruer M, Yildirim G, Varilci A, Terzioglu C. Effect of zirconium diffusion on the microstructural and superconducting properties of $YBa_2Cu_3O_{7-\delta}$ superconductors. J Alloys Compd. 2012;540:260–6.
6. Alibadi A, Farschi YA, Akhavan M. A new Y-based HTSC with T_c above 100 K. Physica C. 2009;469:2012-4.
7. Tavana A, Akhavan M. How T_c can go above 100 K in the YBCO family. Eur Phys J B. 2010;73:79-83.
8. Gholipour S, Daadmehr V, Rezakhani AT, Khosroabadi H, Shahbaz FT, Akbarnejad RH. Structural phase of Y358 superconductor comparison with Y123. J Supercond Nov Magn. 2012;25:2253-8.
9. Khosroabadi H, Rasti M, Akhavan M. Structural analysis of $Y_3Ba_5Cu_8O_{19-\delta}$ High-T_c superconductors by ab initio density function theory. Physica C. 2014;497:84-8.
10. Fujishiro H, Teshima H, Ikebe M, Noto K. Thermal conductivity of YBaCuO bulk superconductors under applied field: effect of content and size of Y211 phase. Physica C. 2003;392–6:171–4.
11. Barnes PN, Haugan TJ, Baca FJ, Varanasi CV, Wheeler R, Meisenkothen F, Sathiraju S. Inducing self-assembly of Y_2BaCuO_5 nanoparticles via Ca-doping for improved pinning in $YBa_2Cu_3O_{7-x}$. Physica C. 2009;469:2029–32.
12. Harnois C, Desgardin G, Laffez I, Chaud X, Bourgault D. High quality weld of melt textured YBCO using Ag doped YBCO junctions. Physica C. 2002;383:269–78.
13. Li AH, Liu HK, Ionescu M, Wang XL, Dou SX, Collings EW, Sumption M, Bhatia M, Lin ZW, Zhu JG. Improvement of critical current density and thermally assisted individual vortex depinning

in pulsed-laser-deposited $YBa_2Cu_3O_{7-\delta}$ thin films on $SrTiO_3$ (100) substrate with surface modification by Ag nanodots. J Appl Phys. 2005;97:1-3.

14. Udomsamuthirun P, Kruaehong T, Nilkamjon T, Ratreng S. The new superconductors of YBaCuO materials. J Supercond Nov Magn. 2010;23:1377-80.
15. Sujinnapram S, Udomsamuthirun P, Kruaehong T, Nilkamjon T, Ratreng S. XRD spectra of new YBaCuO superconductors. Bull Mater Sci. 2011;5:1053-7.
16. Rodriguez-Carvajal J. An introduction to the program FULLPROF [Internet]. France: Laboratoire Leon Brillouin. 2001. Available from: https://www.psi.ch/sites/default/files/import/sinq/dmc/ManualsEN/fullprof.pdf
17. Fisher RA, Gordon J, Phillips NE. Some chemical and structural effect on the properties of high-T_c superconductors. Annu Rev Phys Chem. 1996;47:283–325.
18. Lien CY, Kao HCI, Ling DC, Lu HH, Chen JM, Lee JM. Structure and superconductivity of $Bi_2(Sr_{2-x}M_x)CuO_6$ (M = La, Gd, Y) compounds. Chin J Phys. 2005;43:629-37.
19. Hahn Th. International tables for crystallography, Springer Publication, 262. Netherland. 2004.
20. Sleight AW. Chemistry of high temperature superconductors. Science. 1988;242:1519-27.
21. Choy JH, Chol SY, Byeon SH, Chun SH, Hong ST, Jung DY, Choe WY, Park YW. Determination of the copper valency and oxygen deficiency in the high-T_c superconductor $YBa_2Cu_3O_{7-\delta}$. Bull Korean Chem Soc. 1988;9(5):289-91.
22. Feng J, Lu Y, Zhou L, Zhang P, Xu X, Chen S, Zhang C, Xiong X, Liu G. The study on melting behavior of precursor powders for powder melting processe $YBa_2Cu_3O_{7-x}$ superconductor. Physica C. 2007;459:52-5.